Electronic Supplementary Information

The Influence of Coordination Modes and Active Sites of 5-(Triazol-1-yl) Nicotinic Ligand on Assembly of Diverse Metal-Organic Frameworks: Topology Structures, Gas Sorption Behaviour and Magnetic Properties

Yang-Tian Yan,‡ Si-Si Zhang,‡ Guo-Ping Yang,* Wen-Yan Zhang, Fang Zhang, Feng Cao, Rui-Feng Yang, and Yao-Yu Wang*

Key Laboratory of Synthetic and Natural Functional Molecule Chemistry of the Ministry of Education, Shaanxi Key Laboratory of Physico-Inorganic Chemistry, College of Chemistry & Materials Science, Northwest University, Xi'an 710127, P. R. China

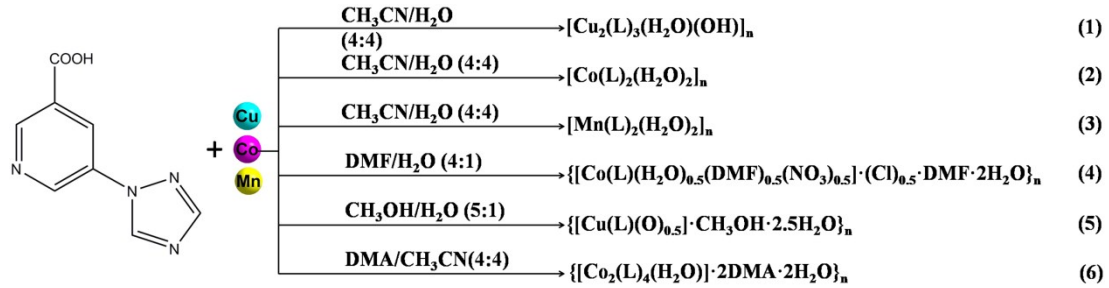

Illustration: Synthesis procedures for complexes **1**-**6**.

Table S1 Selected bond lengths (Å) and bond angles (°) for **1-6.**

Complex **1**			
Cu(1)-O(1)	1.915(5)	Cu(2)-O(2)	2.299(4)
Cu(1)-O(4)	2.025(3)	Cu(2)-O(3)	1.966(3)
Cu(1)-O(7)	1.995(3)	Cu(2)-O(5)	1.956(3)
Cu(1)-N(4)#2	1.988(4)	Cu(2)-N(9)#3	2.071(4)
N(4)-Cu(1)#2	1.988(4)	O(1)-Cu(1)#1	2.449(3)
Cu(1)-O(1)#1	2.449(3)	Cu(2)-O(1)	1.939(3)
O(1)-Cu(1)-O(4)	91.72(13)	O(7)-Cu(1)-O(1)#1	102.14(10)
O(1)-Cu(1)-O(7)	93.58(13)	O(7)-Cu(1)-O(4)	174.48(13)
O(1)-Cu(1)-N(4)#2	176.65(14)	N(4)#2-Cu(1)-O(1)#1	130.43(12)
O(1)-Cu(1)-O(1)#1	87.01(12)	N(4)#2-Cu(1)-O(4)	85.18(14)

O(4)-Cu(1)-O(1)#1	82.46(9)	N(4)#2-Cu(1)-O(7)	89.49(15)
O(1)-Cu(2)-N(9)#3	177.09(14)	O(1)-Cu(2)-O(2)	91.68(13)
O(3)-Cu(2)-O(2)	91.83(14)	O(1)-Cu(2)-O(3)	90.94(13)
O(3)-Cu(2)-N(9)#3	86.62(15)	O(1)-Cu(2)-O(5)	96.88(13)
Cu(2)-O(1)-Cu(1)#1	136.99(15)	Cu(1)-O(1)-Cu(2)	108.17(15)
N(9)#3-Cu(2)-O(2)	86.82(15)	O(5)-Cu(2)-O(2)	96.33(14)
Cu(1)-O(1)-Cu(1)#1	92.99(12)	O(5)-Cu(2)-O(3)	168.51(14)
O(5)-Cu(2)-N(9)#3	85.77(15)		
Symmetrical codes: #1 -x+2, -y+2, -z+1; #2 –x+2, -y+3, z; #3 x-1, y, z; #4 x+1, y, z.			
Complex **2**			
Co(1)-O(3)	2.0809(15)	O(3)#1-Co(1)-O(2)#1	88.00(7)
Co(1)-O(2)#1	2.1143(16)	O(3)-Co(1)-O(2)#1	92.00(7)
Co(1)-O(2)	2.1143(16)	O(3)#1-Co(1)-O(2)	92.00(7)
Co(1)-N(4)#2	2.1511(19)	O(3)-Co(1)-O(2)	88.00(7)
Co(1)-N(4)#3	2.1511(19)	O(2)#1-Co(1)-O(2)	180.0
Co(1)-O(3)#1	2.0809(15)	O(3)#1-Co(1)-N(4)#2	83.11(7)
O(2)#1-Co(1)-N(4)#3	84.17(7)	O(3)-Co(1)-N(4)#2	96.89(7)
O(2)-Co(1)-N(4)#3	95.83(7)	O(2)#1-Co(1)-N(4)#2	95.83(7)
N(4)#2-Co(1)-N(4)#3	180.0	O(2)-Co(1)-N(4)#2	84.17(7)
O(3)-Co(1)-N(4)#3	83.11(7)	O(3)#1-Co(1)-O(3)	180.0
O(3)#1-Co(1)-N(4)#3	96.89(7)	N(4)-Co(1)#4	2.1511 (19)
Symmetrical codes: #1-x+1, -y+2, -z; #2 -x+2, y+1/2, -z+1/2; #3 x-1, -y+3/2, z-1/2; #4 –x+2, y-1/2, -z+1/2.			
Complex **3**			
Mn(1)-O(3)#1	2.1703(19)	Mn(1)-O(3)	2.1705(19)
Mn(1)-O(1)	2.1728(19)	O(3)-Mn(1)-O(3)#1	180.0
Mn(1)-O(1)#1	2.1729(19)	O(3)-Mn(1)-O(1)	88.38(7)
Mn(1)-N(4)#2	2.280(2)	O(3)#1-Mn(1)-O(1)	91.62(7)
Mn(1)-N(4)#3	2.280(2)	O(3)-Mn(1)-O(1)#1	91.62(7)
N(4)-Mn(1)#4	2.280(2)	O(3)#1-Mn(1)-O(1)#1	88.38(7)
O(1)-Mn(1)-N(4)#2	94.84(7)	O(1)-Mn(1)-O(1)#1	180.0
O(1)#1-Mn(1)-N(4)#2	85.15(7)	O(3)-Mn(1)-N(4)#2	97.90(7)
O(3)-Mn(1)-N(4)#3	97.89(7)	O(3)#1-Mn(1)-N(4)#2	94.85(7)
O(3)#1-Mn(1)-N(4)#3	82.11(7)	O(1)#1-Mn(1)-N(4)#3	85.15(7)
O(1)-Mn(1)-N(4)#3	85.16(7)	N(4)#2-Mn(1)-N(4)#3	180.0
Symmetrical codes: #1 -x+1, -y+2, -z; #2 -x+2, y+1/2, -z+1/2; #3 x-1, -y+3/2, z-1/2; #4 –x+2, y-1/2, -z+1/2.			
Complex **4**			
Co(1)-O(3)	2.178(6)	Co(1)-O(4)#1	2.110(5)

Co(1)-O(5)#2	2.072(5)	N(5)#3-Co(1)-O(3)	85.4(3)
Co(1)-O(1)	2.132(5)	O(4)#1-Co(1)-N(5)#3	88.7(2)
Co(1)-N(3)	2.170(6)	O(5)#2-Co(1)-O(4)#1	97.2(3)
Co(1)-N(5)#3	2.159(6)	O(5)#2-Co(1)-O(3)	89.8(3)
O(4)-Co(1)#4	2.110(5)	O(5)#2-Co(1)-O(1)	89.6(2)
O(5)-Co(1)#5	2.072(5)	O(5)#2-Co(1)-N(3)	175.4(3)
O(1)-Co(1)#6	2.132(5)	O(5)#2-Co(1)-N(5)#3	86.1(2)
N(5)-Co(1)#7	2.159(6)	O(1)-Co(1)-O(3)	91.5(3)
O(4)#1-Co(1)-O(3)	170.63(2)	O(1)-Co(1)-N(3)	91.6(2)
O(4)#1-Co(1)-O(1)	94.8(2)	O(1)-Co(1)-N(5)#3	174.78(19)
O(4)#1-Co(1)-N(3)	87.0(3)	N(3)-Co(1)-O(3)	85.4(3)
N(1)-O(1)-Co(1)#6	123.0(2)	N(5)#3-Co(1)-N(3)	92.3(3)
N(1)-O(1)-Co(1)	123.0(2)	Co(1)#6-O(1)-Co(1)	113.7(4)
Symmetrical codes: #1 -x+y-1, -x-1, z-1/3；#2 y, x+1, -z；#3 -x+y-1, -x-1, z+2/3；#4 -y-1, x-y, z+1/3；#5 y-1, x, -z；#6 x-y, -y, -z-1/3; #7 -y-1, x-y, z-2/3.			
Complex **5**			
Cu(1)-O(1)	2.276(5)	N(4)#2-Cu(1)-N(1)#1	92.3(2)
Cu(1)-N(1)#1	2.076(6)	O(2)#3-Cu(1)-O(1)	98.6(2)
Cu(1)-N(4)#2	2.013(6)	O(2)#3-Cu(1)-N(1)#1	168.8(2)
Cu(1)-O(2)#3	1.992(4)	O(2)#3-Cu(1)-N(4)#2	85.1(2)
Cu(1)-O(3)	1.903(4)	O(3)-Cu(1)-O(1)	94.84(18)
N(1)-Cu(1)#4	2.076(6)	O(3)-Cu(1)-N(1)#1	88.8(2)
O(3)-Cu(1)#3	1.903(4)	O(3)-Cu(1)-N(4)#2	175.8(2)
N(1)#1-Cu(1)-O(1)	92.1(2)	O(3)-Cu(1)-O(2)#3	93.02(17)
N(4)#2-Cu(1)-O(1)	89.1(2)	Cu(1)-O(3)-Cu(1)#3	118.4(4)
Symmetrical codes: #1 -x+y+1, -x+1, z+1/3; #2 x, y, z+1; #3 y, x, -z+1; #4 -y+1, x-y, z-1/3; #5 x, y, z-1.			
Complex **6**			
Co(1)-O(1)	2.083(3)	N(5)-Co(1)-O(5)	92.84(13)
O(5)-Co(1)#5	2.144(2)	N(5)-Co(1)-N(1)#2	91.23(16)
Co(1)-O(4)#1	2.071(3)	Co(1)-O(5)-Co(1)#5	114.91(18)
Co(1)-O(5)	2.144(2)	O(4)#1-Co(1)-O(1)	172.69(15)
Co(1)-N(1)#2	2.134(4)	O(4)#1-Co(1)-O(5)	91.17(11)
Co(1)-N(5)	2.118(4)	O(4)#1-Co(1)-N(1)#2	89.65(14)
O(3)-Co(1)#3	2.052(4)	O(4)#1-Co(1)-N(5)	86.44(17)
O(4)-Co(1)#4	2.071(3)	N(1)#2-Co(1)-O(5)	175.89(13)
O(1)-Co(1)-O(5)	91.22(11)	O(1)-Co(1)-N(1)#2	88.45(13)
O(1)-Co(1)-N(5)	86.54(16)		

Symmetrical codes: #1 –y+1, x-y, z-1/3; #2 y+1, -x+y+1, z-1/3; #3 x-y, x, z+1/3; #4–x+y+1, -x+1, z+1/3; #5 -x+1, -y, z.

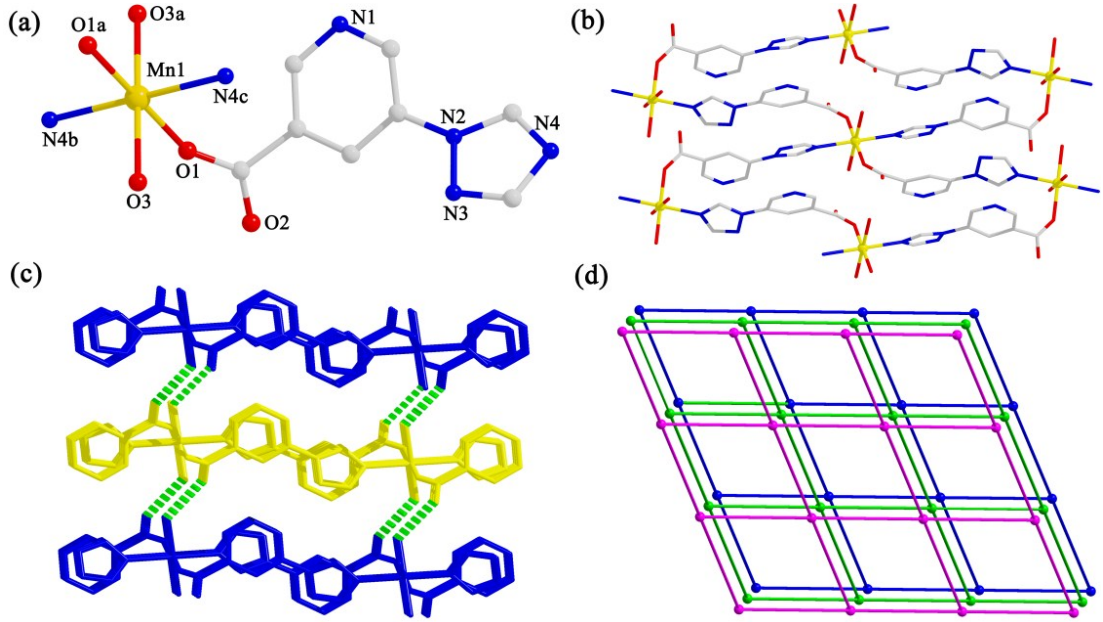

Fig. S1 (a) Coordination environment around the Mn(II) ions in **3**. Symmetry codes: a: 1-x, 2-y, -z; b: -1+x, 1.5-y,-0.5+z; c: 2-x, 0.5+y, 0.5-z. (gray C, red O, blue N, yellow Mn); (b) 2D layers structure in **3**. (c) The hydrogen bonds between the adjacent layers. (d) The uninodal 4-connected ***sql*** net for **3**.

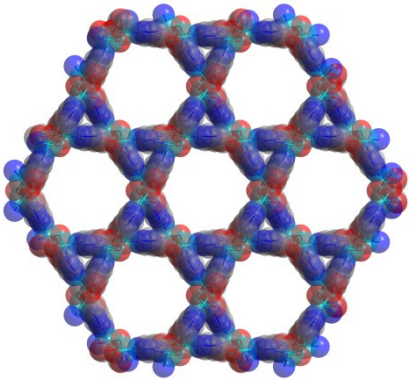

Fig. S2 3D microporous framework of **5** and the hexagon shape of 1D channel along *c* axe. All the H atoms and guest molecules are omitted for clarity.

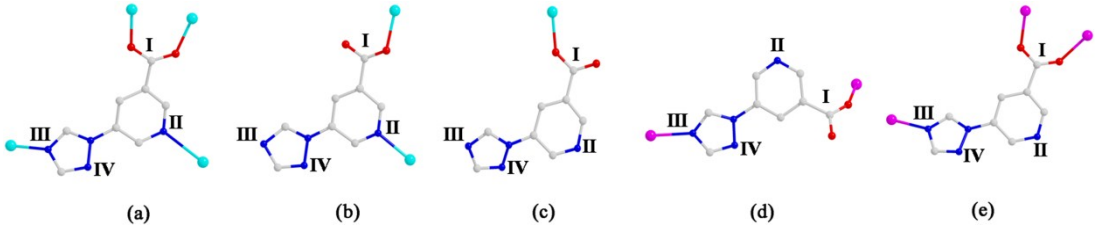

Fig. S3 Coordination modes of H_5L in **1-6**.

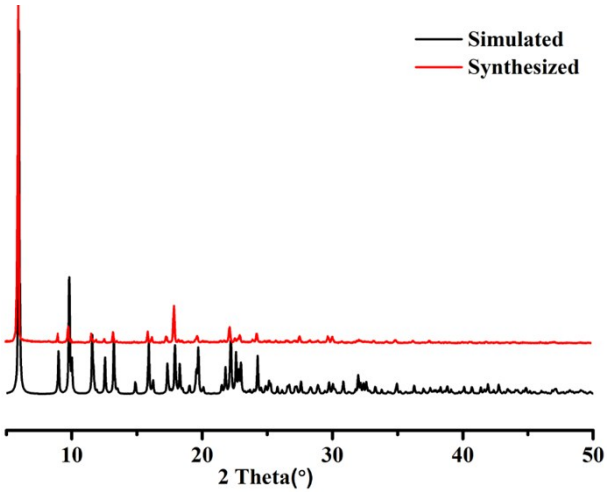
Simulated
Synthesized
10
20
30
40
50
2 Theta(°)

(a)

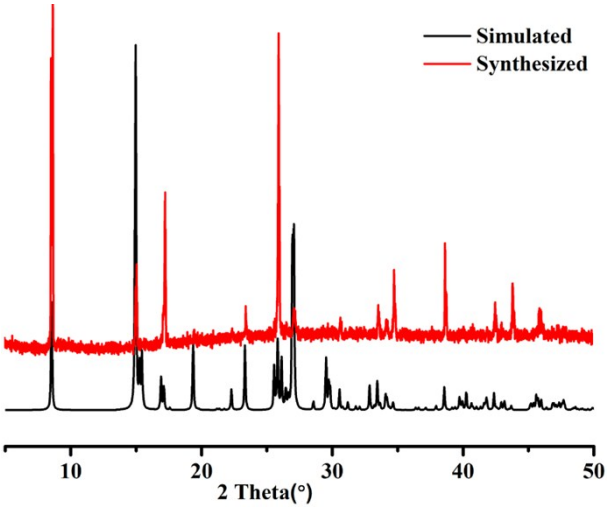
Simulated
Synthesized
10
20
30
40
50
2 Theta(°)

(b)

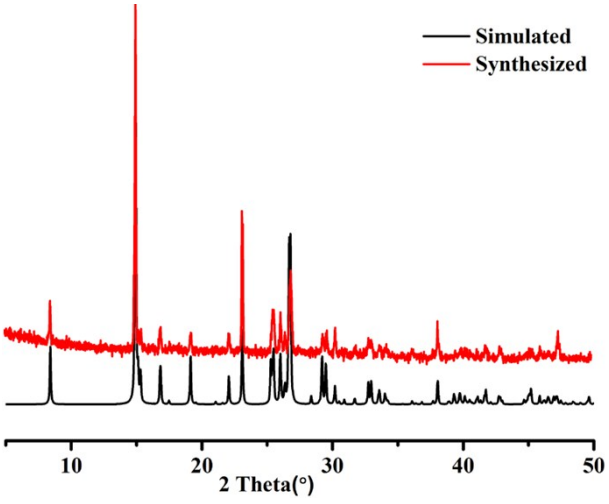
Simulated
Synthesized
10
20
30
40
50
2 Theta(°)

(c)

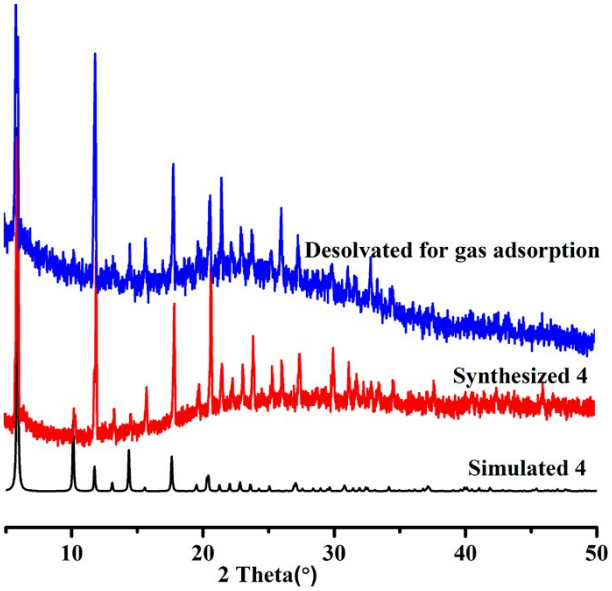

(d)

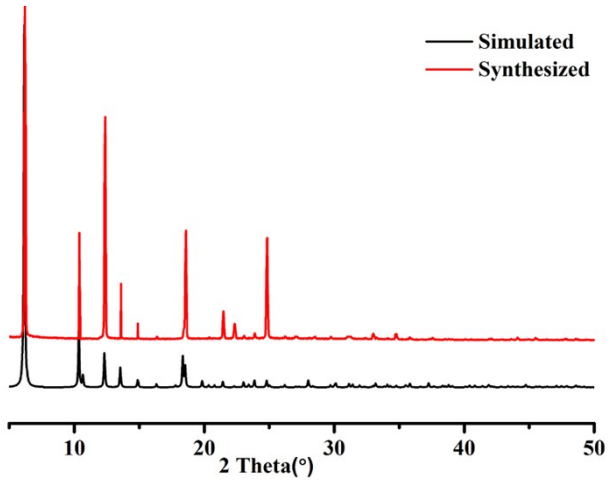

(e)

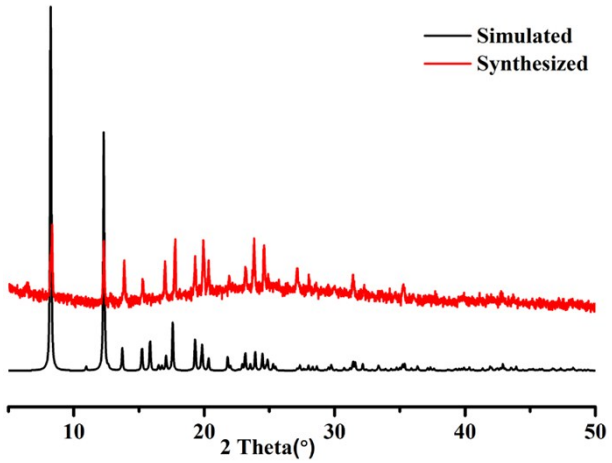

(f)

Fig. S4 PXRD patterns of **1**-**6** in (a-f) simulated from the X-ray single-crystal structure, experimental samples and desolvated samples.

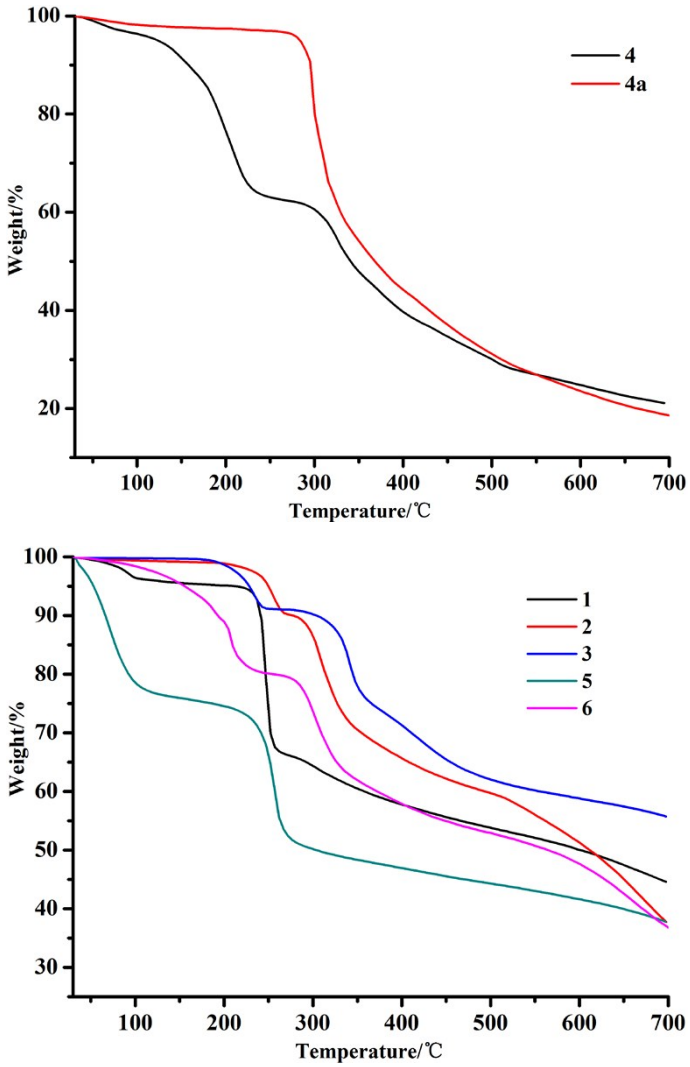

Fig. S5 TGA plots of complexes **1-6.**

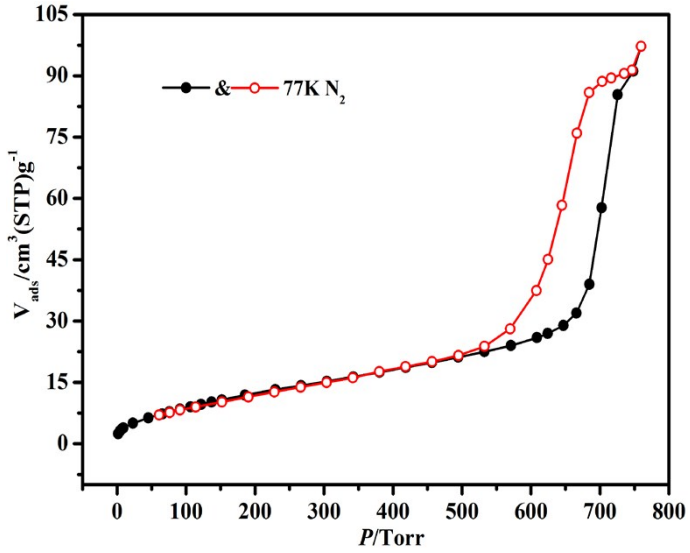

Fig. S6 N_2 adsorption and desorption isotherm at 77K of **4a.**

IAST adsorption selectivity calculation

The experimental isotherm data for pure CO_2, CH_4 and N_2 (measured at 273 and 298 K) were fitted using a Langmuir-Freundlich (L-F) model

$$q = \frac{a * b * p^c}{1 + b * p^c}$$

Where q and p are adsorbed amounts and pressures of component i, respectively. The adsorption selectivities for binary mixtures of CO_2/CH_4 at 273 and 298 K and CO_2/N_2 at 298 K, defined by

$$S_{ads} = (q_1 / q_2) / (p_1 / p_2)$$

Where qi is the amount of i adsorbed and pi is the partial pressure of i in the mixture.

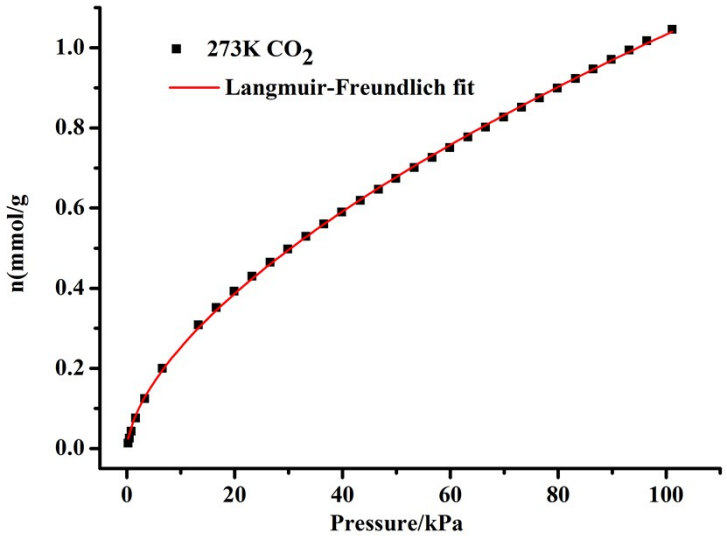

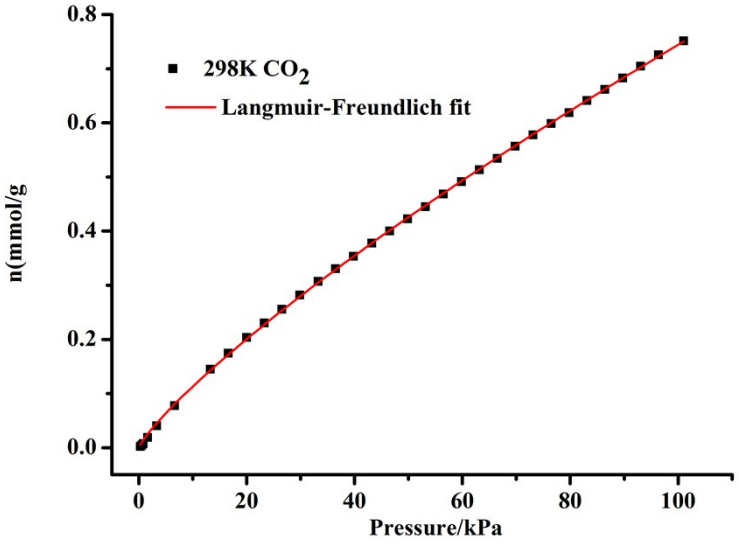

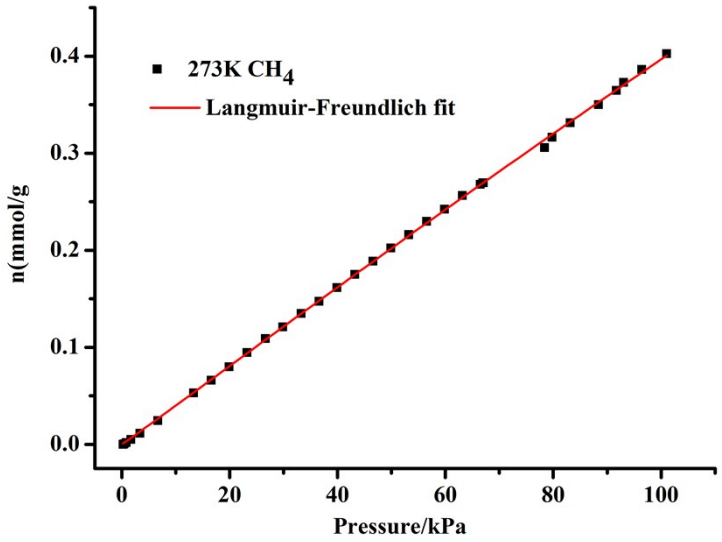
273K CH4
Langmuir-Freundlich fit
n(mmol/g
Pressure/kPa
0.0
0.1
0.2
0.3
0.4
0
20
40
60
80
100

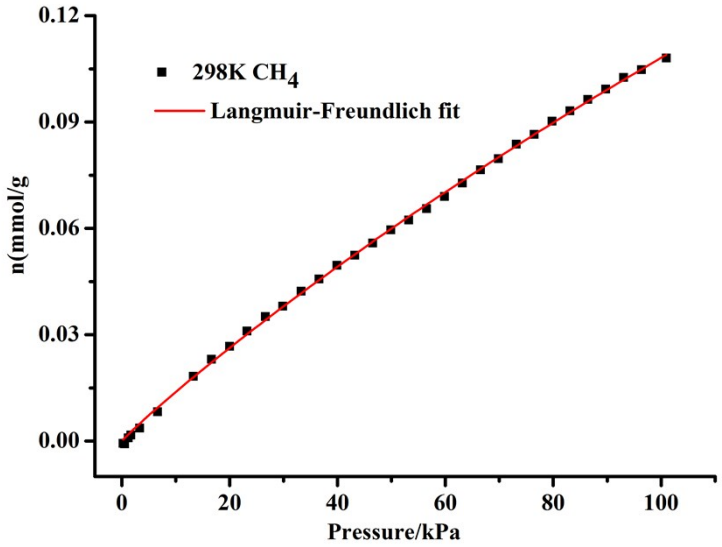
298K CH4
Langmuir-Freundlich fit
n(mmol/g
Pressure/kPa
0.00
0.03
0.06
0.09
0.12
0
20
40
60
80
100

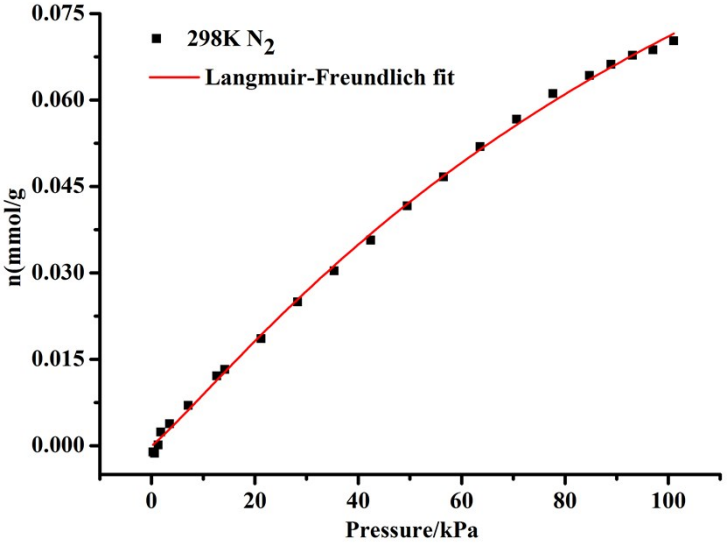

Fig. S7 CO_2 adsorption isotherms of **4a** at 273 K with fitting by L-F model: a = 41.89057, b = 0.00145, c =0.62074, Chi^2 = 3.65 $\times 10^{-5}$, R^2 = 0.99963; CO_2 adsorption isotherms of **4a** at 298 K with fitting by L-F model: a = 15.38937, b = 0.00107, c =0.83754, Chi^2 = 8.91 $\times 10^{-6}$, R^2 = 0.99984; CH_4 adsorption isotherms of **4a** at 273K with fitting by L-F model: a = 5.65559, b = 6.68 $\times 10^{-4}$, c =1.02627, Chi^2 = 4.44 $\times 10^{-6}$, R^2 = 0.99973; CH_4 adsorption isotherms of **4a** at 298 K with fitting by L-F model: a = 0.81106, b = 0.00196, c = 0.94703, Chi^2 = 6.51 $\times 10^{-7}$, R^2 = 0.99947; N_2 adsorption isotherms of **4a** at 298 K with fitting by L-F model: a = 0.0225, b = 3.15 $\times 10^{-4}$, c = 1.11251, Chi^2 = 9.16 $\times 10^{-7}$, R^2 = 0.99871.

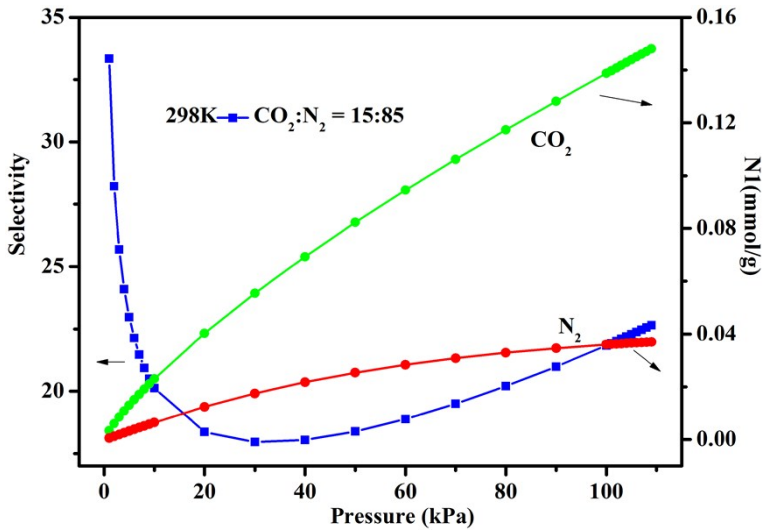

Fig. S8 IAST adsorption selectivity of **4a** for the CO_2/N_2 mixtures with 15:85 components at 298 K.

Calculation of sorption heat for CO_2 uptake using Virial 2 model

$$\ln P = \ln N + 1/T \sum_{i=0}^{m} aiN^i + \sum_{i=0}^{n} biN^i \quad Q_{st} = -R \sum_{i=0}^{m} aiN^i$$

The above equation was applied to fit the combined CO_2 isotherm data for desolvated **4a** at 273 and 298 K, where P is the pressure, N is the adsorbed amount, T is the temperature, ai and bi are virial coefficients, and m and n are the number of coefficients used to describe the isotherms. Q_{st} is the coverage-dependent enthalpy of adsorption and R is the universal gas constant.

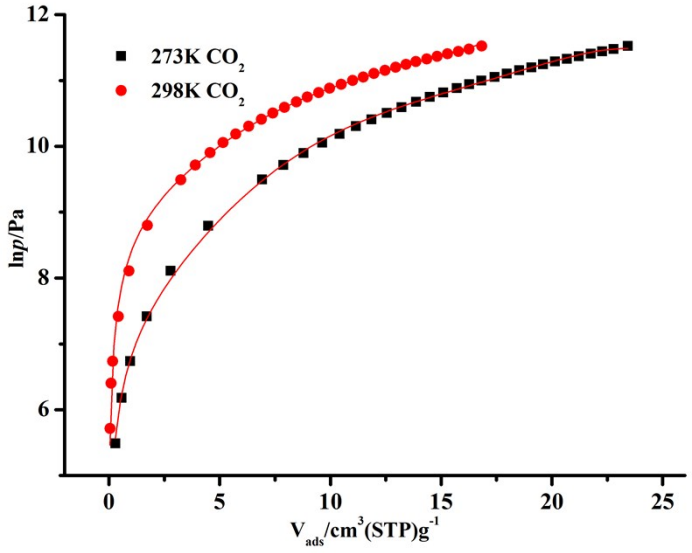

Fig. S9 Virial analysis of the CO_2 adsorption data at 273 and 298 K for **4a**. Fitting results: a0= -5636.56569, a1 = 432.87858, a2 = -1.14691, a3 = -1.48544, a4 = 0.06519, Chi^2 = 0.00403, R^2 = 0.99838.

Magnetic properties of 1, 2, 4, 5 and 6

The antiferromagnetic properties of **1**, **2**, **4**, **5** and **6** are briefly discussed as below. As shown in Fig. S10a, the $\chi_M T$ of **1** at room temperature is 0.96 cm^3 K mol^{-1}, which is in fair agreement with the theoretical value (0.75 cm^3 K mol^{-1}) calculated from two Cu(II) ions(S= 1/2, g=2). Upon cooling, the $\chi_M T$ starts to slowly decrease to 18 K, and then sharply decreases to 0.24 cm^3 K mol^{-1} at 2K, indicating the antiferromagnetic interactions between Cu ions. The temperature dependence of the reciprocal susceptibilities ($1/\chi_M$) of **1** is fitted from 25 K to 300 K, which obeys the Curie–Weiss law, $\chi_M = C/(T - \theta)$, with $\theta = -6.38$ K and $C = 1.20$ cm^3 K mol^{-1}. The negative θ value manifests the presence of antiferromagnetic interactions among tetranuclear Cu(II) ions.[1]

For **2**, the $\chi_M T$ at room temperature is 2.97 cm^3 K mol^{-1} (Fig. S10b), which is greatly larger than the spin-only value (1.875 cm^3 K mol^{-1}) for one isolated Co(II) ion (S =3/2), resulting from the significant orbital contribution of high-spin Co(II)ion. Upon cooling, the $\chi_M T$ continuously decreases to 0.95 cm^3 K mol^{-1} at 2 K, which is ascribed to the antiferromagnetic interactions between Co(II) ions. The temperature dependence of the reciprocal susceptibilities ($1/\chi_M$) of **2** obeys the Curie–Weiss law, the best-fit parameters for the Curie–

Weiss model in the temperature region of 25 ~ 300 K gives $\theta = -15.96$ K and $C = 3.11$ cm^3 K mol^{-1}. The negative θ value indicates the antiferromagnetic interactions among adjacent Co(II) ions.[2]

For **4**, the $\chi_M T$ at room temperature is 3.05 cm^3 K mol^{-1} (Fig. S10c), which is greatly larger than the spin-only value (1.875 cm^3 K mol^{-1}) for one isolated Co(II) ion (S =3/2), resulting from the significant orbital contribution of high-spin Co(II) ion. Upon cooling, the $\chi_M T$ continuously decreases to 1.10 cm^3 K mol^{-1} at 2 K, which is ascribed to the antiferromagnetic interactions between Co(II) ions. The temperature dependence of the reciprocal susceptibilities ($1/\chi_M$) of **4** obeys the Curie–Weiss law, the best-fit parameters for the Curie–Weiss model in the temperature region of 100~ 300 K gives $\theta = -5.96$ K and $C = 3.15$ cm^3 K mol^{-1}. The negative θ value indicates the antiferromagnetic interactions among adjacent Co(II) ions.

For **5**, the $\chi_M T$ at room temperature is 0.35 cm^3 K mol^{-1} (Fig. S10d), which is close to the theoretical value (0.375 cm^3 K mol^{-1}) calculated from one Cu(II) ion (S= 1/2, g=2). Upon cooling, the $\chi_M T$ starts to slowly decrease to 0.02 cm^3 K mol^{-1} at 2 K, indicating the antiferromagnetic interactions between Cu ions. The temperature dependence of the reciprocal susceptibilities ($1/\chi_M$) of **5** is fitted from 120 K to 300 K, which obeys the Curie–Weiss law with $\theta = -458.04$ K and $C = 0.90$ cm^3 K mol^{-1}. The negative θ value manifests the presence of antiferromagnetic interactions among Cu(II) ions.

For **6**, the $\chi_M T$ at room temperature is 5.98 cm^3 K mol^{-1} (Fig. S10e), which is greatly larger than the spin-only value (3.75 cm^3 K mol^{-1}) for two Co(II) ions (S =3/2), resulting from the significant orbital contribution of high-spin Co(II) ion. Upon cooling, the $\chi_M T$ continuously decreases to 0.22 cm^3 K mol^{-1} at 2 K, which is ascribed to the antiferromagnetic interactions between Co(II) ions. The temperature dependence of the reciprocal susceptibilities ($1/\chi_M$) of **6** obeys the Curie–Weiss law, the best-fit parameters for the Curie–Weiss model in the temperature region of 100~ 300 K gives $\theta = -25.34$ K and $C = 6.54$ cm^3 K mol^{-1}. The negative θ value indicates the antiferromagnetic interactions among adjacent Co(II) ions.

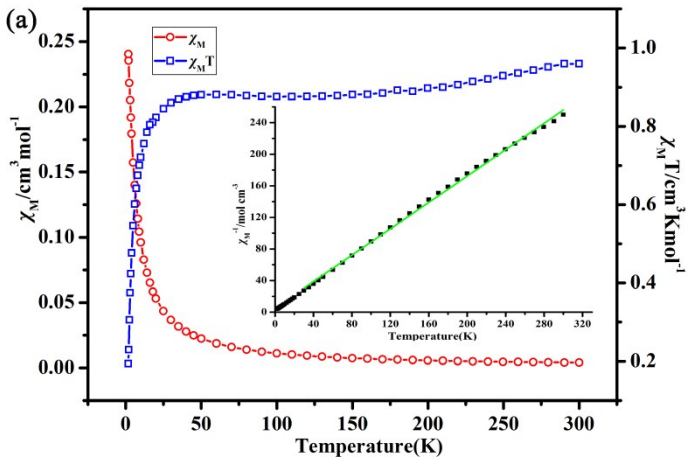

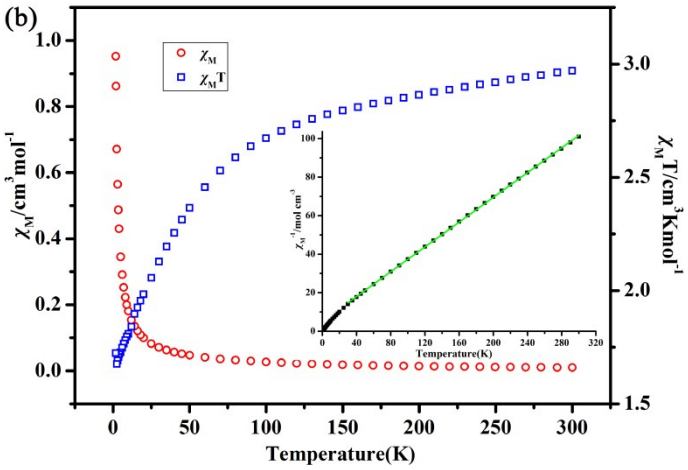
(b)
χM
χMT
χM/cm3mol-1
χMT/cm3Kmol-1
Temperature(K)
χM-1/mol cm-3
Temperature(K)

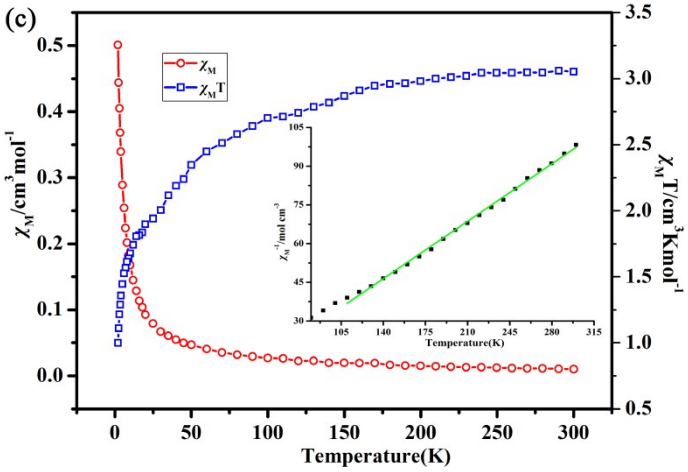
(c)
χM
χMT
χM/cm3mol-1
χMT/cm3Kmol-1
Temperature(K)
χM-1/mol cm-3
Temperature(K)

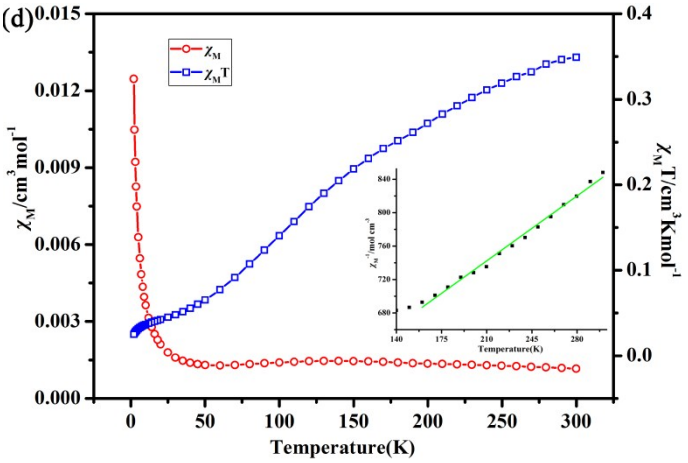
(d)
χM
χMT
χM/cm3mol-1
χMT/cm3Kmol-1
Temperature(K)
χM-1/mol cm-3
Temperature(K)

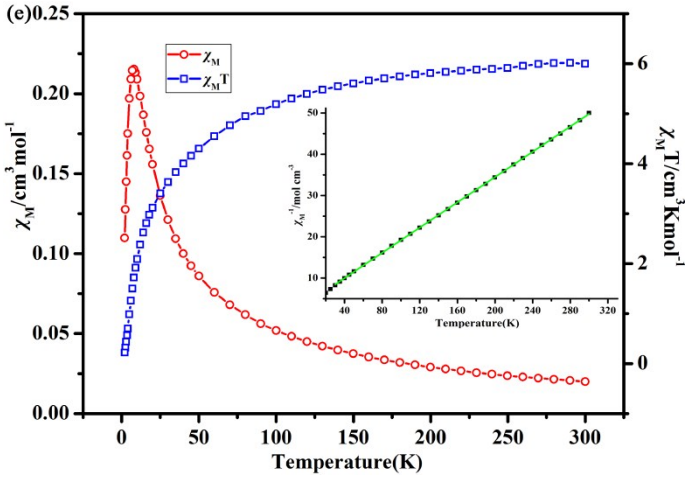

Fig. S10 The $\chi_M T$, χ_M, and $1/\chi_M$ vs. T plots of **1**, **2**, **4**, **5** and **6** in (a-e), respectively. The green line represents the fits.

Reference

1 (a) D. W. Ryu, W. R. Lee, K. S. Lim, W. J. Phang, C. S. Hong, *Cryst. Growth Des.*, 2014, **14**, 6472−6477. (b) S. Bala, S. Bhattacharya, A. Goswami, A. Adhikary, S. Konar, R. Mondal, *Cryst. Growth Des.*, 2014, **14**, 6391−6398.

2 (a) Z. Chen, B. Zhao, P. Cheng, X. Q. Zhao, W. Shi, Y. Song, *Inorg. Chem.*, 2009, **48**, 3493−3495. (b) Q.-J. Zhang, B.-H. Li, L. Chen, *Inorg. Chem.*, 2013, **52**, 9356−9362. (c) D.-M. Chen, X.-Z. Ma, X.-J. Zhang, N. Xu, P. Cheng, *Inorg. Chem.*, 2015, **54**, 2976−2982. (d) X.-Y. Liu, L. Sun, H.-L. Zhou, P.-P. Cen, X.-Y. Jin, G. Xie, S,-P. Chen, Q.-L. Hu, *Inorg. Chem.*, 2015, **54**, 8884−8886.

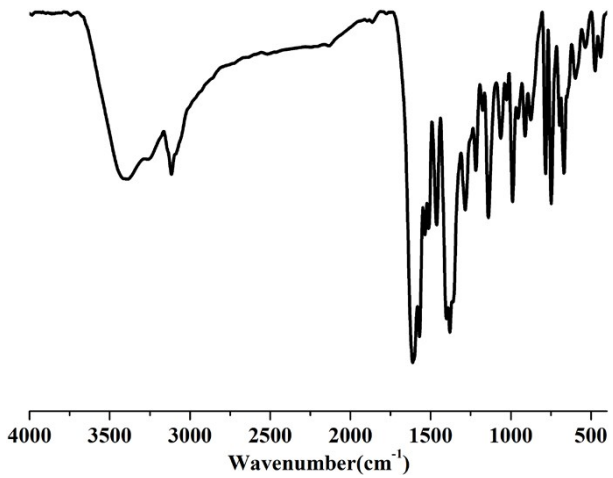

(a)

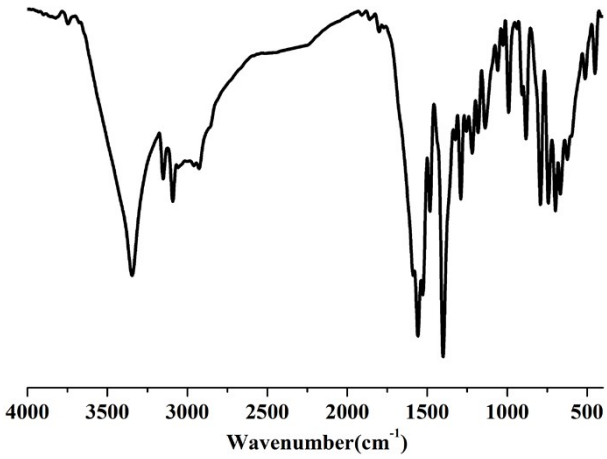
4000
3500
3000
2500
2000
1500
1000
500
Wavenumber(cm-1)

(b)

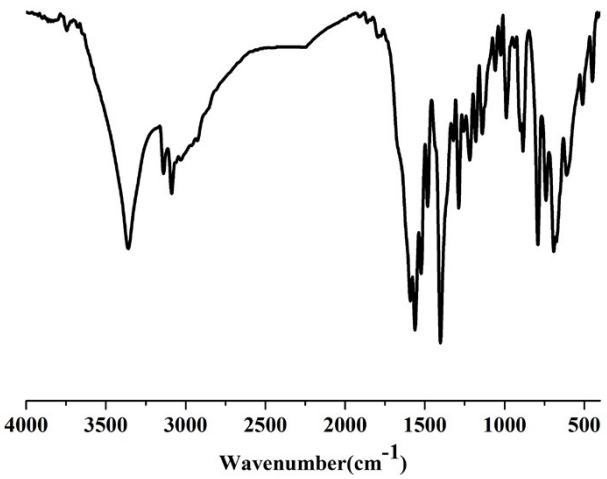
4000
3500
3000
2500
2000
1500
1000
500
Wavenumber(cm-1)

(c)

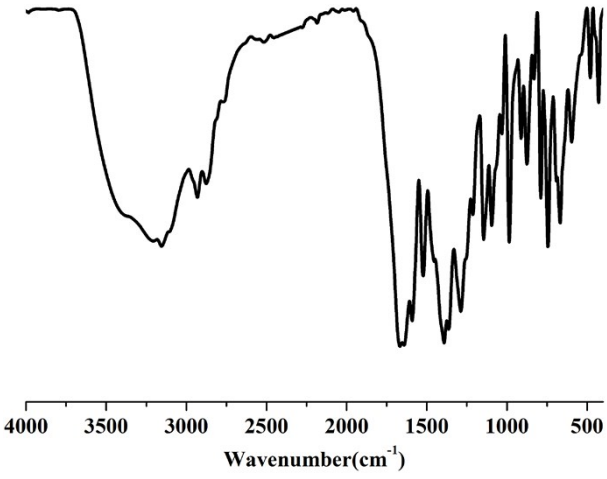
4000
3500
3000
2500
2000
1500
1000
500
Wavenumber(cm-1)

(d)

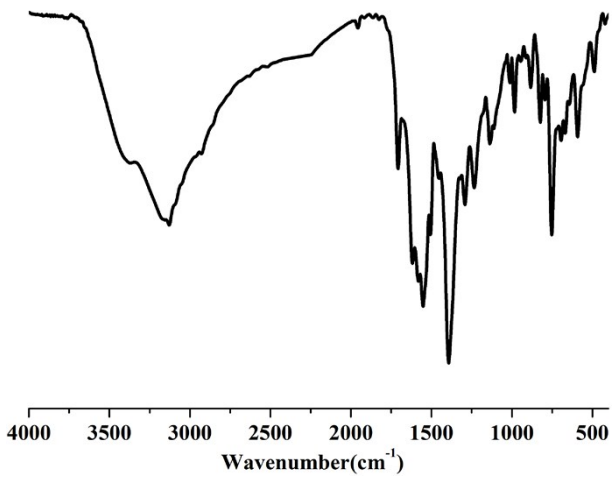

(e)

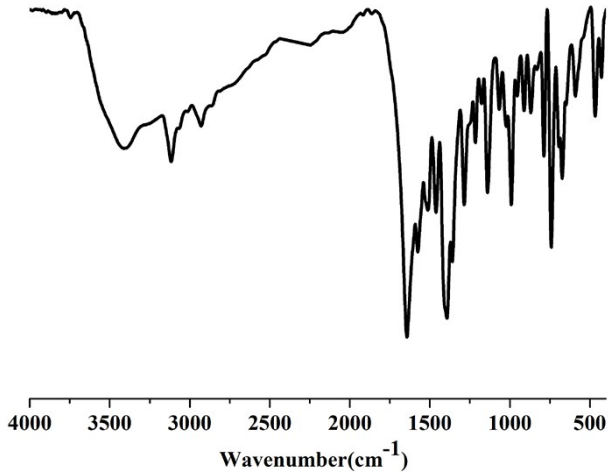

(f)

Fig. S11 IR spectra of the as-synthesized **1-6** in (a-f).